Propagation of an optical beam in a photorefractive medium in the presence of a photogalvanic nonlinearity or an externally applied electric field

A. A. Zozulya and D. Z. Anderson
Joint Institute for Laboratory Astrophysics, University of Colorado and National Institute of Standards and Technology, Boulder, Colorado 80309-0440

(Received 4 May 1994; revised manuscript received 29 July 1994)

We consider propagation of a light beam in photorefractive media in the framework of a three-dimensional model. We formulate equations governing three-dimensional distribution of a nonlinear refractive index. The distributions of electric charge, potential, current, refractive index, and the near- and far-field output intensities of the beam are calculated. The conditions necessary for observing self-focusing in photorefractive media are discussed.

PACS number(s): 42.65.Hw, 42.50.Ne

I. INTRODUCTION

Propagation of a light beam through a nonlinear medium is accompanied by a series of complex changes in its spatiotemporal structure. A theoretical interpretation of these phenomena is of key importance for gaining insight into the nonlinear properties of a particular medium and for contributing to our understanding of more general questions of complex spatiotemporal behavior of nonlinear systems. Photorefractive media are a type of nonlinear media potentially promising for optical data processing [1,2]. The nonlinearity exhibited by these media differs from the conventional Kerr-type nonlinear response in many important ways. First, it is intrinsically nonlocal in nature and second, many features of nonlinear beam mixing in such media are almost independent of the intensities of the interacting beams, which determine only the characteristic relaxation time scales. In addition, the photorefractive response can also be controlled by externally applied ac or dc electric fields [1,2].

The physics of propagation of a single light beam through a photorefractive medium is a topic of ongoing research in photorefractive nonlinear optics. Previous theoretical analyses [3–6] have concentrated mostly on the case of no photogalvanic effect and/or an applied electric field (see, e.g., the two-dimensional analysis in Ref. [6] and references therein). In the present paper we formulate full three-dimensional equations governing distribution of the nonlinear refractive index, induced by a single optical beam in a photorefractive medium. They explicitly take into account the anisotropic nature of the medium and allow for the presence of a photogalvanic nonlinearity and/or an externally applied electric field. The structure of the equations is essentially that of a nonlinear electrostatic problem. Their solution involves calculation of a long-range electrostatic potential and requires proper imposition of asymptotic boundary conditions. The most important parameter in these equations is the value of the normalized dark intensity. This parameter is the ratio of the rate of thermal excitation of carriers to the rate of photoexcitation determined by a characteristic intensity of the beam. We show that propagation of the beam through the medium is accompanied by the generation of macroscopic steady-state vortex currents. We also calculate and analyze distributions of electric charge, potential, refractive index, and output near- and far-field intensity distribution of the beam, and discuss conditions for self-focusing in photorefractive media.

II. FORMULATION OF THE PROBLEM

Material response of a photorefractive medium is governed by the set of equations [7]

$$\frac{\partial}{\partial t}N_D^+=(\beta+sI_{\rm em})(N_D-N_D^+)-\xi n_e N_D^+ , \tag{1a}$$

$$\nabla\cdot(\epsilon_0\hat{\epsilon}\mathbf{E})=\rho , \tag{1b}$$

$$\frac{\partial}{\partial t}\rho+\nabla\cdot\mathbf{J}=0 , \tag{1c}$$

$$\rho=e(N_D^+-N_A-n_e) , \tag{1d}$$

$$\mathbf{J}=e\mu n_e\mathbf{E}+\mu\kappa_B T\nabla n_e+\beta_{\rm ph}(N_D-N_D^+)\mathbf{c}I_{\rm em} . \tag{1e}$$

Here N_D, N_D^+, N_A, and n_e are the density of donors, ionized donors, acceptors, and conducting electrons, respectively; β and s are the thermal and photoexcitation coefficients; $I_{\rm em}$ is the intensity of electromagnetic radiation, ξ is the recombination constant, $\mathbf{E}$ is the amplitude of the static electric field, e is the elementary charge, ϵ_0 the electric permeability of vacuum, $\hat{\epsilon}$ is the static dielectric tensor; ρ and $\mathbf{J}$ are the charge and the electric current densities, respectively, μ is the electron mobility, κ_B is the Boltzmann constant, and T is the temperature. The photogalvanic tensor is assumed to have the largest component $\beta_{\rm ph}$ generating current along the direction of the axis of spontaneous polarization of the medium (axis $\mathbf{c}$), and other components are neglected.

In Eqs. (1) the characteristic spatial scale of change of the electric field is determined by the value of the Debye wave number $k_D=(e^2N_A/\kappa_B T\epsilon_0\epsilon_c)^{1/2}$, and the characteristic value of this field is determined by $\tilde{E}=\kappa_B Tk_D/e\equiv eN_A/\epsilon_0\epsilon_c k_D$, where ϵ_c is the component

of the static dielectric tensor along the c axis. The characteristic density of electrons associated with electromagnetic intensity I_0 is equal to $n_0 = sI_0(N_D - N_A)/\xi N_A$ and the characteristic relaxation time of the electric field is $t_0 = \epsilon_0 \epsilon_c / e\mu n_0$. We introduce the dimensionless densities of the ionized donors $N = N_D^+ / N_A$ and the electrons $n = n_e / n_0$, and define the dimensionless potential of the static electric field φ by the relation $\nabla\varphi = -k_D \mathbf{E}/\tilde{E}$. Finally we introduce the dimensionless intensity of the electromagnetic radiation, which includes a contribution from the thermal excitation of carriers: $I = (I_{\rm em} + \beta/s)/I_0 \equiv \tilde{I}_{\rm em} + I_d$, where I_0 is some characteristic intensity (e.g., in the center of the beam). The term I_d will be referred to as the normalized dark intensity. In typical conditions $I_d \ll 1$, so this last term is often neglected; for the problem we are considering, its proper treatment is of extreme importance. The presence of I_d and its value will determine most of the physics to be discussed below.

Using the functions defined above and under the standard assumption of $N_A \gg n_e$, we see that Eqs. (1) may be rewritten in the form

$$\delta \frac{\partial}{\partial \tau} N = I[1 + \chi k_D^{-2} \nabla \cdot (\hat{\epsilon}_n \nabla \varphi)] - nN \ , \tag{2a}$$

$$k_D^{-2} \nabla \cdot (\hat{\epsilon}_n \nabla \varphi) = 1 - N \ , \tag{2b}$$

$$\nabla \cdot \left[\frac{\partial}{\partial \tau} \hat{\epsilon}_n \nabla \varphi + n \nabla \varphi - \nabla n - c k_D [1 + \chi k_D^{-2} \nabla \cdot (\hat{\epsilon}_n \nabla \varphi)] \frac{E_{\rm ph}}{\tilde{E}} \tilde{I}_{\rm em} \right] = 0 \ , \tag{2c}$$

where $\tau = t/t_0$, $\delta = \mu e / \epsilon_0 \epsilon_c \xi$ is the ratio of the characteristic relaxation time of the donor density to that of the potential, $\chi = N_A/(N_D - N_A)$, $\hat{\epsilon}_n$ is the static dielectric tensor divided by ϵ_c, and $E_{\rm ph} = \beta_{\rm ph} \xi N_A / e\mu s$ is the photogalvanic field.

In typical conditions, $\delta \ll 1$. Thus $\delta \approx (0.1-2) \times 10^{-4}$ for $LiNbO_3$ and $\delta \approx (0.01-1) \times 10^{-2}$ for $BaTiO_3$ using data given in Refs. [8,9]. Also, in a majority of cases of practical interest, $k_D^{-2} \nabla \cdot (\hat{\epsilon}_n \nabla \varphi) \ll 1$. This inequality breaks down for very small diameters of the beam and for very large values of the photogalvanic and/or an applied electric field; analysis of such a situation is outside the scope of the present paper. Under the above assumptions Eqs. (2) can be reduced to one equation for the potential φ:

$$I^{-1} \frac{\partial}{\partial \tau} \nabla \cdot (\hat{\epsilon}_n \nabla \varphi) + \nabla^2 U(\varphi, I) + \nabla \ln I \cdot \nabla U(\varphi, I) - k_D \frac{E_{\rm ph}}{\tilde{E}} \mathbf{c} \cdot \nabla \ln I = 0 \ , \tag{3}$$

where

$$U(\varphi, I) = \varphi - k_D^{-2} \nabla \cdot (\hat{\epsilon}_n \nabla \varphi) - \ln I \ . \tag{4}$$

The electric current $\mathbf{J}$ under the same assumptions is given by the relation

$$\mathbf{J} = -I \nabla U(\varphi, I) + \mathbf{c} k_D \frac{E_{\rm ph}}{\tilde{E}} (I - I_d) \tag{5}$$

(recall that $I = \tilde{I}_{\rm em} + I_d$).

The amplitude $B(\mathbf{r})$ of an electromagnetic beam propagating in a photorefractive medium obeys the equations [7]

$$\left[\frac{\partial}{\partial l} - \frac{i}{2k} \nabla_\perp^2 - i\nu \right] B(\mathbf{r}) = 0 \ , \tag{6}$$

$$\nu(\mathbf{r}) = \frac{k}{2k_D} n^2 \tilde{E} \mathbf{e}_p \cdot (\hat{r}_{\rm el} \cdot \nabla \varphi) \cdot \mathbf{e}_p \ , \tag{7}$$

where l is a direction of propagation of the beam, $\nabla_\perp^2$ is a Laplace operator acting on coordinates perpendicular to this direction, $k = 2\pi n/\lambda$ (n is the index of refraction) is the wave number of electromagnetic radiation in the medium, $\hat{r}_{\rm el}$ is the electro-optic tensor, and $\mathbf{e}_p$ is the unity vector in the direction of polarization of the beam. The function ν determined by relation (7) is simply the normalized nonlinear addition to the refractive index of the medium. The intensity of light $I_{\rm em}$ entering into Eqs. (3) and (4) equals $|B(\mathbf{r})|^2$.

The boundary conditions for Eqs. (3) and (4) depend on the physics of the interaction. Thus in the case of no externally applied electric field and nonconducting crystal faces they may correspond to zero normal components of electric current at the crystal faces: $\mathbf{J}_{\rm norm} = 0$. If the characteristic beam diameter is considerably less than the size of the crystal the condition $\mathbf{J}_{\rm norm} = \mathbf{0}$ applies to the entrance and exit faces of the crystal. Side faces may be moved to infinity and the boundary conditions $\mathbf{J}_{\rm norm} = \mathbf{0}$ replaced by the requirement that the electrostatic potential φ and, consequently, the function U, tend to (different) constants when moving in the direction of these faces. Once the function U is known, the potential φ is found by solving Eq. (4), which, in principle, requires matching the solution of an outer electrostatic problem for the potential with that inside the crystal. In practice, this does not cause difficulties. Equation (4) contains the spatial screening scale k_D^{-1}, which is very small. A simple analysis shows that the influence of the boundaries (i.e., the particular boundary conditions at the input and the output faces of the crystal) becomes small at distances exceeding several k_D^{-1}. Note that Eq. (3) does not have such an independent scale. The characteristic scales of change in function U are determined by those of the light beam, which are in general considerably larger. In this sense, proper boundary conditions are more important for Eq. (3) than for Eq. (4).

III. PROPERTIES OF SOLUTIONS

In the following we analyze steady-state solutions for Eqs. (3) and (4). We consider the following geometry of interaction: the crystal is cut along crystallographic axes, the beam is polarized along the axis z, propagates along the axis x, enters at the face $x = 0$, and exits at $x = L$. The side faces of the crystal are at infinity (the diameter of the beam is much smaller than the size of the crystal) and the photogalvanic current is generated along the z

axis (**c** is parallel to the z axis). The external electric field (if any) is also applied along the z axis. According to Eq. (7) the nonlinear refractive index may be due to either r_{zzy} (r_{32}) or r_{zzz} (r_{33}) components of the electro-optic tensor. We assume that the corresponding component is r_{33} as is the case in $LiNbO_3$, for example. Relation (7) in this case reads $\nu(\mathbf{r})=(k/2)n^2 r_{33}\tilde{E}G(\mathbf{r})$, where $G(\mathbf{r})=k_D^{-1}\partial\varphi(\mathbf{r})/\partial z$. Since $\nu(\mathbf{r})\propto G(\mathbf{r})$, in the following we shall refer to function G as the normalized nonlinear refractive index. This function is simply the normalized amplitude of the z component of the static electric field **E**.

First we show that both the photogalvanic nonlinearity and the nonzero applied electric field in the open circuit configuration can be treated in a unified way. Indeed, suppose we have the potential difference V between two faces of the crystal perpendicular to the axis z. In the absence of the beam this potential difference would correspond to the field $E_{\text{ext}}=-V/L_z$ directed along z (L_z is the size of the crystal along z). The boundary conditions for the potential φ correspond to $\varphi(z=L_z/2)=k_D V/2\tilde{E}$, $\varphi(z=-L_z/2)=-k_D V/2\tilde{E}$. The appearance of k_D and $\tilde{E}$ in the previous relation is connected to our choice of normalization for φ. Instead of functions φ and U obeying Eqs. (3) and (4) we introduce the renormalized functions $\varphi_n=\varphi+k_D(E_{\text{ext}}/\tilde{E})z$ and $U_n=U+k_D(E_{\text{ext}}/\tilde{E})z$. The equation for U_n reads as

$$I^{-1}\frac{\partial}{\partial\tau}\nabla\cdot(\hat{\epsilon}_n\nabla\varphi_n)+\nabla^2 U_n(\varphi_n,I)+\nabla\ln I\cdot\nabla U_n(\varphi_n,I)-k_D\frac{E_{\text{ext}}+E_{\text{ph}}}{\tilde{E}}\mathbf{c}\cdot\nabla\ln I=0\ . \quad (8)$$

Note that Eq. (8) has the same form as Eq. (3). The function $U_n(\varphi_n,I)$ is still determined by Eq. (4) with the replacements $\varphi\to\varphi_n$, $U\to U_n$. If boundaries of the medium are at infinity (the size of the crystal is considerably larger than the characteristic diameter of the beam), the boundary conditions for φ_n and U_n along transverse directions correspond to those functions tending to constants when their arguments tend to infinity. After solving for φ_n, the electrostatic potential φ is obtained through the relation $\varphi=\varphi_n-k_D(E_{\text{ext}}/\tilde{E})z$. The structure of Eq. (8) shows that the photogalvanic nonlinearity is analogous to the applied electric field.

If there is no photogalvanic nonlinearity and no applied external electric field, the solution of Eq. (3) yields $U(\varphi,I)=0$. Note that this solution corresponds to the absence of current in the crystal: $\mathbf{J}=\mathbf{0}$. The case of nonzero photogalvanic nonlinearity and/or applied electric field is more interesting. Consider the situation in which the intensity of the beam is radially symmetric: $I(x,y,z)=I(r_\perp)$, where $r_\perp=\sqrt{y^2+z^2}$. The structure of Eq. (8) then immediately reveals that its solution in the steady state should have the form $U_n(x,y,z)=(E_{\text{ext}}+E_{\text{ph}})\tilde{E}^{-1}k_D z F(r_\perp)$, where the function F obeys the equation

$$r_\perp F''+[3+r_\perp(\ln I)']F'+(\ln I)'(F-1)=0 \quad (9)$$

and the primes denote differentiation with respect to $r_\perp$. The boundary conditions for Eq. (9) are $F(r_\perp=0)$ is finite and $F(r_\perp\to\infty)\to 0$.

Consider the solution of Eq. (9) for a Gaussian beam $I(r_\perp)=\exp(-8r_\perp^2/d^2)+I_d$. A small I_d allows one to use the approximation $(\ln I)'\approx -16r_\perp/d^2$ for $r_\perp<r_*$ and $(\ln I)'\approx 0$ for $r_\perp>r_*$, where $r_*^2=(d^2/8)\ln I_d^{-1}$. The solution of Eq. (9) then takes the form

$$F=\begin{cases}1-c_1 M\left[\frac{1}{2},2;\eta=\frac{8r_\perp^2}{d^2}\right], & \eta<\eta_* \quad (10a)\\ c_2\eta^{-1}, & \eta>\eta_* \quad (10b)\end{cases}$$

where $\eta_*=8r_*^2/d^2=\ln I_d^{-1}$, $M(\frac{1}{2},2;\eta)$ is the Kummer function, and c_1,c_2 are constants. Using asymptotics of the Kummer function for large arguments $M(\frac{1}{2},2;\eta)\approx\pi^{-1/2}\eta^{-3/2}\exp(\eta)$ and matching (10a) and (10b) we find $c_1=\sqrt{\pi\eta_*}\exp(-\eta_*)$ and $c_2=\eta_*(1-\eta_*^{-1})$. The Taylor expansion of the Kummer function at small values of its argument is $M(\frac{1}{2},2;\eta)\approx 1+\eta/4+\cdots$, so function F in the central region of the beam ($8r_\perp^2/d^2\le 1$) has the form

$$F(r_\perp)\approx 1-8\alpha I_d\frac{r_\perp^2}{d^2}+\cdots\ , \quad (11)$$

where $\alpha=\sqrt{\pi\ln I_d^{-1}}/4$.

If we know the function F and the distribution of intensity I, we can determine the distribution of current **J**. It is given by

$$\mathbf{J}=\mathbf{c}k_D\frac{E_{\text{ext}}+E_{\text{ph}}}{\tilde{E}}I[1-F(r_\perp)]-\mathbf{c}k_D\frac{E_{\text{ph}}}{\tilde{E}}I_d-\frac{\mathbf{r}_\perp}{r_\perp}k_D\frac{E_{\text{ext}}+E_{\text{ph}}}{\tilde{E}}IzF'(r_\perp)\ . \quad (12)$$

Equation (1c) in the steady state reads as $\nabla\cdot\mathbf{J}=\mathbf{0}$. According to Eq. (12), in the absence of the photorefractive nonlinearity and the applied electric field, this means $\mathbf{J}=\mathbf{0}$. For nonzero values of E_{ext} and/or E_{ph} this is no longer true and $\mathbf{J}\neq\mathbf{0}$. The relation $\nabla\cdot\mathbf{J}=\mathbf{0}$ implies that the current has a vortex structure and loops on itself. The current should generate a magnetic field. This situation is well known in plasma physics, for example, where such magnetic fields result in anomalous transport properties of plasma (see, e.g., [10]). In photorefractive media the magnetic field is small and may be neglected.

Having calculated the function U_n we are in a position to find the electrostatic potential from Eq. (4). In typical conditions the characteristic diameter of the beam is much larger than the inverse Debye wave number, so that the second term in this equation containing derivatives is relatively small and for the purposes of a qualitative analysis may be neglected. The distribution of the potential then is governed by the relation

$$\varphi(y,z)=\ln I(r_\perp)+\frac{E_{\text{ext}}+E_{\text{ph}}}{\tilde{E}}k_D z F(r_\perp)-\frac{E_{\text{ext}}}{\tilde{E}}k_d z\ , \quad (13)$$

where function F obeys Eq. (9). Equation (13) shows that

the electrostatic potential consists of three terms, and that both the photogalvanic nonlinearity and the applied field contribute to the potential additively. The first term $\ln I$ for a radially symmetric light beam is symmetric in z, whereas the second term proportional to $zF(r_\perp)$ is antisymmetric. The nonlinear refractive index is proportional to $\partial\varphi/\partial z$. The contribution from the first term will be antisymmetric in z whereas the second term will give a symmetric contribution. The third term will give a uniform addition to the refractive index.

For a Gaussian beam in the region where $I \gg I_d$, the z derivative of $\ln I$ in Eq. (13) gives a refractive index that varies linearly across the beam. This results in a bending of the beam trajectory toward the c axis. An explanation of this phenomenon in the framework of a two-dimensional model and in the absence of the photogalvanic nonlinearity and/or an applied electric field has been given in Ref. [3]. The term $\ln I$ is also responsible for asymmetric amplification of a spatially broadband noise (fanning) [11]. The relative contribution of this term to the refractive index becomes larger for smaller diameters of the beam.

The second term in Eq. (13) may result in a self-focusing or defocusing of a light beam, but only if the dark intensity I_d is not very small. Indeed, substituting Eq. (11) into Eq. (13) results in the following expression for the potential φ:

$$\varphi(y,z)\approx -\frac{8r_\perp^2}{d^2}+\frac{E_{\rm ext}+E_{\rm ph}}{\tilde{E}}k_D z\left[1-8\alpha I_d\frac{r_\perp^2}{d^2}\right] -\frac{E_{\rm ext}}{\tilde{E}}k_D z\ . \tag{14}$$

The refractive index (7) according to Eq. (14) is given by the expression

$$\nu(y,z)\approx -k\frac{z}{l_b}-\alpha\frac{k}{2}\frac{3z^2+y^2}{l_{\rm NL}^2}+\tfrac{1}{2}kn^2E_{\rm ph}r_{33}\ , \tag{15}$$

where $l_b=k_D d^2/8n^2r_{33}\tilde{E}$ and $l_{\rm NL}^2=d^2/8n^2r_{33}(E_{\rm ext}+E_{\rm ph})I_d$.

The last term in Eq. (15) gives a uniform renormalization of the refractive index and may be ignored. Since $l_{\rm NL}^2\propto I_d^{-1}$, the limit of zero dark intensity $I_d\to 0$ corresponds to vanishing of the second term. Hence, despite nonzero values of $E_{\rm ph}$ and $E_{\rm ext}$, their contribution to the nonuniform part of the refractive index equals zero. The physical reason for this phenomenon is the screening of the photogalvanic nonlinearity and/or the applied electric field by a redistribution of charges. The relevant physics will be discussed in more detail in Sec. IV. Note that the dark intensity in the case of an applied electric field may also include any additional erasure intensity. Our results indicate that to observe steady-state self-focusing or self-defocusing of a light beam in a photorefractive medium it may be advantageous to illuminate the crystal with an additional expanded light beam incoherent to the primary one. Note also that Eq. (15) corresponds to a steady state. The situation may be different in the transient regime when the redistribution of charges is still incomplete. Since the characteristic relaxation time of the potential is inversely proportional to the local intensity [see Eq. (8)], the buildup of the refractive index is faster in the highly illuminated regions of the beam. This means that even if the steady-state self-focusing or defocusing is impossible, one may observe some focusing or defocusing in the transient regime.

Previous analysis shows that the structure of the potential φ in the general three-dimensional case is relatively complex. Some useful insight may be gained by resorting to a two-dimensional model, i.e., by considering only one transverse coordinate z. Solution of Eq. (8) in this case is trivial and, assuming that the characteristic diameter of the beam is much less than the transverse size of the medium, is given by the expression

$$U_n(z)=\frac{E_{\rm ph}+E_{\rm ext}}{\tilde{E}}k_D\left[z-\int^z dz'\frac{I_d}{I}\right]\ . \tag{16}$$

Substituting Eq. (16) into Eq. (4) results in the following expression for the potential φ:

$$\varphi(z)-k_D^{-2}\frac{\partial^2}{\partial^2 z^2}\varphi(z)=\ln I+\frac{E_{\rm ph}}{\tilde{E}}k_D z -\frac{E_{\rm ph}+E_{\rm ext}}{\tilde{E}}k_D\int^z dz'\frac{I_d}{I}\ . \tag{17}$$

Equation (17) explicitly demonstrates the effect of screening of the external electric field and shows that the term responsible for self-focusing or self-defocusing of the beam is directly proportional to the value of the dark intensity I_d. To make further progress we may use the standard aberrationless approximation and consider the amplitude of the beam in the medium of the form

$$B(x,z)=\frac{1}{\sqrt{f(x)}}\exp\left[-4\frac{[z-z_0(x)]^2}{d^2f^2(x)} +i\frac{k}{2}[z-z_0(x)]^2\frac{f'}{f} +ik\theta(x)z+ik\psi(x)\right]\ . \tag{18}$$

Here d is the initial diameter of the beam and f, z_0, θ, and ψ are functions depending only on the longitudinal direction of propagation x; a prime denotes differentiation with respect to this coordinate. The product $df(x)$ is the local coordinate-dependent diameter of the beam in the medium, z_0 is the position of its center, $R(x)=f/f'$ is the radius of curvature, and $\theta(x)$ is the angle of the tilt of the wave front with respect to axis x. The initial conditions correspond to $f(x=0)=1$, $z_0(0)=0$, and $\theta(0)=0$.

Substituting the intensity corresponding to the field (18) into the expression for the nonlinear refraction index (7), Taylor expanding around the maximum of the intensity and keeping only terms up to the second order, assuming that the characteristic diameter of the beam is much larger than the inverse Debye wave number, and discarding coordinate-independent terms, one gets [compare to (15)]

$$v(z)\approx-\frac{k}{16}\frac{d^2}{l_{\rm NL}^2}f-k\frac{z-z_0}{l_b f^2}-\frac{k}{2}\frac{(z-z_0)^2}{l_{\rm NL}^2 f}\ . \tag{19}$$

Substituting Eqs. (18) and (19) into the electromagnetic equation (6) and matching terms up to second order in the transverse coordinate z results in the set of equations

$$\frac{d^2}{dx^2}f-\frac{1}{l_d^2 f^3}+\frac{1}{l_{\rm NL}^2}=0\ , \tag{20a}$$

$$z_0(x)=-\frac{1}{l_b}\int_0^x dx'\int_0^{x'}\frac{dx''}{f^2(x'')}\ , \tag{20b}$$

$$\theta(x)=\frac{d}{dx}z_0(x)=-\frac{1}{l_b}\int_0^x\frac{dx'}{f^2(x')}\ , \tag{20c}$$

where $l_d=kd^2/8$ is the characteristic diffraction length of the beam.

The physical meaning of the above equations is quite transparent: in propagating through the medium the beam is changing its diameter in accordance with Eq. (20a). These changes are governed by the diffraction length l_d and the nonlinear refraction length $l_{\rm NL}$. The square of the nonlinear refraction length $l_{\rm NL}^2$ may be either positive or negative depending on the sign of the product $r_{33}(E_{\rm ext}+E_{\rm ph})$. The positive sign corresponds to nonlinear focusing and the negative to defocusing of the beam. Equation (20b) shows that as it is focusing or defocusing, the beam is bending toward the optical axis of the crystal. The magnitude of the transverse displacement z_0 is governed by the nonlinear bending length l_b. Note that l_b is independent of either the external or the photogalvanic field, i.e., the bending takes place in any photorefractive medium. Finally, the local tilt of the wave front $\theta(x)$ is equal to the derivative of the displacement, as demonstrated by Eq. (20c), i.e., the plane component of the wave front is perpendicular to the local direction of propagation. Equations (20) in the limit $l_{\rm NL}^2\to\infty$ were discussed in Ref. [4].

The first integral of Eq. (20a) for an initially collimated beam $[f(x=0)=1, f'(x=0)=0]$ has the form

$$\left[\frac{df}{dx}\right]^2=\frac{(f-1)}{l_d^2 f^2}(1+f-2Pf^2)\ , \tag{21}$$

where $P=l_d^2/l_{\rm NL}^2$.

Equation (21) shows that in the defocusing case $P<0$ ($l_{\rm NL}^2<0$) the diameter of the beam monotonically grows with the longitudinal coordinate x. In the focusing case $P>0$ ($l_{\rm NL}^2>0$) the diameter is a periodic function of the longitudinal coordinate x bounded by two limiting values:

$$f_1=1\ , \tag{22a}$$

$$f_2=\frac{1}{4P}(1+\sqrt{1+8P})\ . \tag{22b}$$

The first (f_1) of these limiting values corresponds to the beam diameter equal to its initial value at the entrance to the medium. The second (f_2) is larger than the initial diameter for $P<1$ and smaller for $P>1$. They become equal (self-channeling) for $l_d=l_{\rm NL}$ ($P=1$) or, equivalently, for $d=2\sqrt{2}/k\sqrt{n^2 r_{33}(E_{\rm ext}+E_{\rm ph})I_d}$.

The aberrationless approximation can also be used to analyze the first stage of evolution of an initial radially symmetric Gaussian beam in the three-dimensional case. According to Eq. (15) the refraction index created by such a beam is not radially symmetric. In the aberrationless approximation the beam becomes elliptical in propagating through the medium and should be characterized by two diameters, $d_y(x)\equiv f_y(x)d$ and $d_z(x)\equiv f_z(x)d$, giving its widths along y and z axes, respectively. For an initially collimated beam $f_y(x=0)=f_z(x=0)=1$, $f_y'(x=0)=f_z'(x=0)=0$; using Eq. (15) and repeating the steps analogous to those of the two-dimensional model, we find the following expressions for the normalized diameters f_y and f_z, the transverse displacement z_0, and the local tilt of the wave front θ, as functions of the longitudinal coordinate x:

$$f_y(x)=1+\left[\frac{1}{l_d^2}-\frac{\alpha}{l_{\rm NL}^2}\right]\frac{x^2}{2}\ , \tag{23a}$$

$$f_z(x)=1+\left[\frac{1}{l_d^2}-3\frac{\alpha}{l_{\rm NL}^2}\right]\frac{x^2}{2}\ , \tag{23b}$$

$$z_0(x)=-\frac{x^2}{2l_b}\ , \tag{23c}$$

$$\theta(x)=-\frac{x}{l_b}\ . \tag{23d}$$

These formulas are valid for $|f_y-1|\ll 1$ and $|f_z-1|\ll 1$. Note that the refractive index is proportional only to the z component of the electrostatic field, so one might think that the nonlinearity would not affect propagation of the beam along the transverse coordinate y at all. This is indeed the case for the part of the refractive index that is independent of either $E_{\rm ph}$ or $E_{\rm ext}$ and is responsible for the bending of the beam, but is not true for the part that is due to the presence of an applied electric field and/or the photogalvanic nonlinearity. The reason is the global nature of the electrostatic problem as described by the elliptic equation (8). Indeed, the functional form of the solution $U_n\propto zF(r_\perp)$ for a radially symmetric beam follows from the boundary condition $U_n(y\to\infty, z\to\infty)\to z$ that should be fulfilled along any direction in the (y,z) plane. Analogously, determining the behavior of function F near the center of the beam [Eq. (11)] involves using a boundary condition for this function at infinity $F(r_\perp\to\infty)\to 0$. Ironically, in one-dimensional plane-wave analyses the part of the refractive index due to the presence of an external electric field usually is referred to as a "local response." In our analysis this part is expressed by the function U_n. The above discussion demonstrates that finding U_n is the most unforgiving intrinsically global part of the problem of calculating the refractive index in the three-dimensional treatment.

The physics described by Eq. (23) is qualitatively similar to that of the two-dimensional model (20). The new part is the explicit description of the anisotropic nature of self-focusing in the three-dimensional case. As before,

changes in the diameters of the beam are determined by the relative values of the diffraction length l_d and the nonlinear refraction length l_{NL}. For negative l_{NL}^2 and for positive l_{NL}^2 such that $l_{NL}^2 \geq 3\alpha l_d^2$ the beam initially diverges along both transverse directions; if $3\alpha l_d^2 \geq l_{NL}^2 \geq \alpha l_d^2$ it experiences focusing along the z axis, but still diverges along the y axis. Finally, if $\alpha l_d^2 \geq l_{NL}^2$, the beam is self-focusing along both transverse directions [one should keep in mind that Eq. (23) describes only the initial stage of evolution].

The above examples allow one to get a feeling for the parameters governing propagation of the beam in a photoreflective medium in the presence of the external electric field and/or the photogalvanic nonlinearity. One of their limitations is that Eqs. (20) and (23) describe propagation of the beam reasonably well only when the value of the dark intensity I_d is relatively high. In the opposite case, the quadratic expansion of the refractive index is insufficient and the aberrationless approximation is a bad choice. This issue will be addressed in Sec. IV.

IV. NUMERICAL RESULTS

We now present numerical solutions of the above equations describing the material response of the photorefractive medium together with the parabolic Maxwell equation for the amplitude of the light beam. As is clear from Sec. III, all the results pertain equally to both the photorefractive nonlinearity and the applied electric field with certain evident modifications.

Figure 1 shows lines of current surrounding a light beam for the case of a photogalvanic nonlinearity and no applied electric field. The calculations were carried out for the Gaussian beam $\tilde{I}_{em}=\exp[-8(r_\perp/d)^2]$ with the beam diameter $d=0.1$ mm. The dark intensity equals 10^{-3}, the Debye wave number $k_D/k_0=k_D\lambda/2\pi=0.66$,

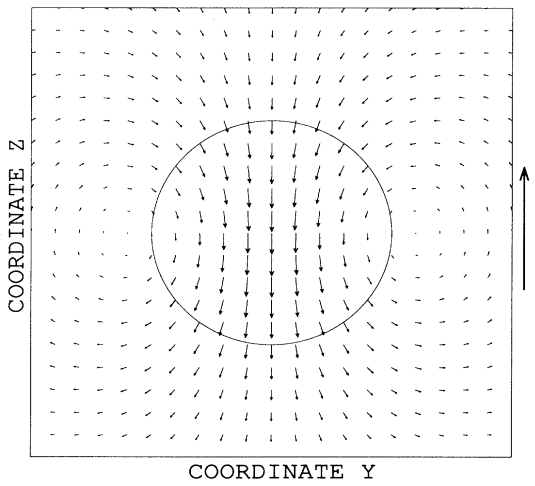

FIG. 1. Distribution of current in the cross section of a Gaussian beam propagating through a medium with photogalvanic nonlinearity. The diameter of the beam $d=0.1$ mm, $E_{ph}/\tilde{E}=-5$, $I_d=10^{-3}$, $k_D/k_0=0.66$. The circle of diameter d shows the position of the beam, the arrow indicates the direction of the **c** axis.

$\lambda=0.514$ μm, $n=2.2$, and $E_{ph}=-5\tilde{E}$. The equation $\nabla\cdot\mathbf{J}=0$ implies that the current has a vortex structure and loops on itself, as indeed is seen in the figure. The negative sign of E_{ph} means that the current created by the photogalvanic term $\mathbf{c}(E_{ph}/\tilde{E})(I-I_d)$ in Eq. (5) flows in the negative direction of the **c** axis. This photogalvanic current results in a redistribution of charges, creating an electrostatic field. The field generates a second current [first term in Eq. (5)], which tries to counterbalance the current created by the photogalvanic term. In other words, the redistribution of charges tries to block the photogalvanic nonlinearity. The current shown in Fig. 1 is the net remaining current as a result of this process. The amplitude of this current is small. The maximum current created by the photogalvanic nonlinearity in the center of the beam equals -5 and the maximum value of the current in Fig. 1 equals -0.02. If the sign of the photogalvanic field E_{ph} is reversed, the distribution of current also changes sign. The distribution of current created by a beam for zero photogalvanic field and nonzero applied electric field is very similar to that shown in Fig. 1. Generation of the current loops by the photogalvanic nonlinearity has been discussed also in Ref. [12].

The charge density distribution created by the beam for the parameters of Fig. 1 is shown in Fig. 2(a); the cross section of the charge density along axis z is depicted in Fig. 2(b). Parts of Fig. 2(a) above the plane correspond to positive charge densities. The arrow indicates the direction of the **c** axis. The distribution shown in Fig. 2(a) is symmetric along the y coordinate and asymmetric along the z coordinate. Note that the charges accumulate in a circular region where the intensity of light becomes comparable to the dark intensity. For the chosen parameters ($I_d=10^{-3}$) this corresponds to a circle of diameter $\approx 2d$ as is clearly seen in Fig. 2(b).

The distributions of the electrostatic potential φ and the cross section of this distribution along axis z are shown in Figs. 3(a) and 3(b), respectively. The values of the principal components of the normalized dielectric tensor $\hat{\epsilon}$ for Figs. 3(a) and 3(b) are equal to $\hat{\epsilon}_z=1$ and $\hat{\epsilon}_y=2$. Note the long-range nature of this distribution that reaches far beyond the region occupied by the bulk of the energy of the beam. Large absolute values of the potential are related to our choice of normalization and should not be surprising in light of the fact that the static electric field is determined by the relation $\mathbf{E}=-(\tilde{E}/k_D)\nabla\varphi$. The potential changes on the scale of the beam diameter d, so $E\propto\tilde{E}\varphi/k_D d$ ($k_D d\gg 1$).

The distribution of the refractive index $G(\mathbf{r})$ and its cross sections along axes z and y are shown in Figs. 4(a)–4(c). As is seen from these figures, the value of G in the central region of the beam is very close to $-E_{ph}/\tilde{E}$, which is to be expected. Indeed, the redistribution of charges almost blocks the photogalvanic term and hence creates the electric field equal to $-E_{ph}$. The distribution of the refractive index $G(\mathbf{r})$ may be visualized as a strong nonparabolic lens, induced by the beam in the medium. The central part of this lens corresponds to negative changes in the refractive index, whereas peripheral regions along the z axis produce positive additions to the

refractive index. The cross section along the y axis shows only negative changes. This character of the distribution of the refractive index was experimentally observed in Ref. [13] using a probe beam with a diameter considerably smaller than that of the primary beam. Our analysis bears out the phenomenological model developed in Ref. [13] to explain this phenomenon.

Propagation of a light beam through such a medium results in changes in its spatial distribution and Fourier spectrum. In Fig. 5 we show the output Fourier power spectrum (equivalent to the far-field intensity distribution) of the input Gaussian beam after it has propagated through a photorefractive medium with the photogalvanic nonlinearity for the previous values of parameters. The cross sections of this spectrum along axes z and y are shown in Figs. 5(b) and 5(c), respectively. All three graphs are plotted on the logarithmic scale. The dashed curves in Figs. 5(b) and 5(c) represent the input Fourier spectrum of the beam. The near-field output intensity distribution of the beam is not much different from the input one and is not shown. The length of the medium equals $L=3$ mm and $kn^2r_{33}\tilde{E}L=4$. Figures 5(a), 5(b), and 5(c) were obtained by direct numerical solution of Eqs. (3), (4), and (6). The spatial derivatives along the direction of propagation x in Eqs. (3) and (4) were neglected as compared to those along y and z. This assumption is justified by the small divergence of the beam in the medium.

Figure 5 illustrates that, in general, changes in the Fourier spectrum of the beam cannot be described in terms of simple focusing or defocusing but rather should be characterized as broadening. This is because the nonlinear lens created by the beam is strongly nonparabolic. Thus for the parameters of Fig. 2 the central part of the refractive-index distribution is almost flat, which means that the central region of the beam does not experience any appreciable lensing, whereas the wings of the beam propagate through regions with strong gradients of the refractive index (the question of what parameters determine the shape and the width of the refractive-index distribution will be discussed in more detail below). Changing the sign of E_{ph} inverts the distributions of the refractive index shown in Fig. 4, but the output Fourier spectrum (far-field intensity distribution) of the beam looks very similar to that shown in Fig. 5. In both cases the output Fourier spectrum of the beam has two symmetric petals aligned along the c axis (see Fig. 5). This picture is qualitatively similar to that usually seen when a light beam propagates through a piece of $LiNbO_3$, but the

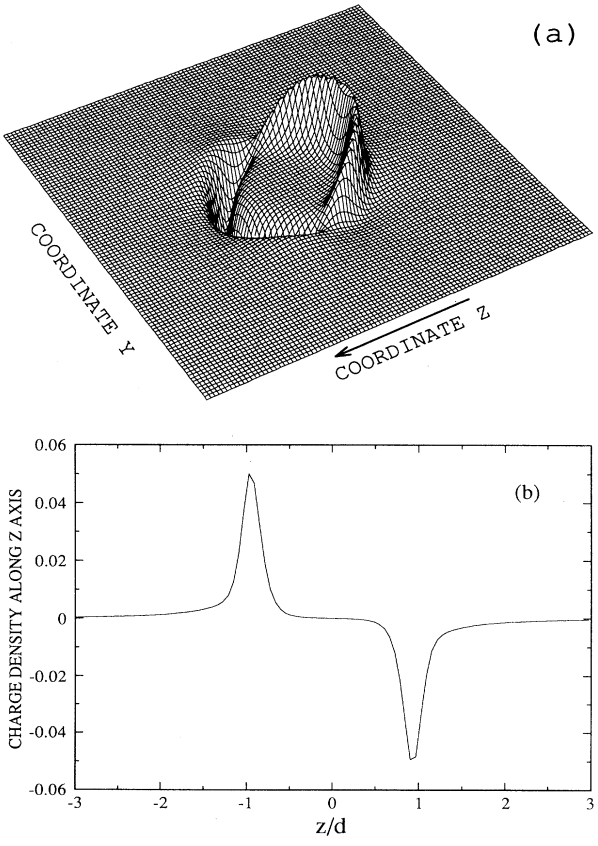

FIG. 2. Charge density distribution created by a Gaussian beam for the parameters of Fig. 1 (a), and its cross section along axis z (b). The arrow indicates the direction of the c axis. The size of the picture in (a) is equal to six beam diameters along either direction.

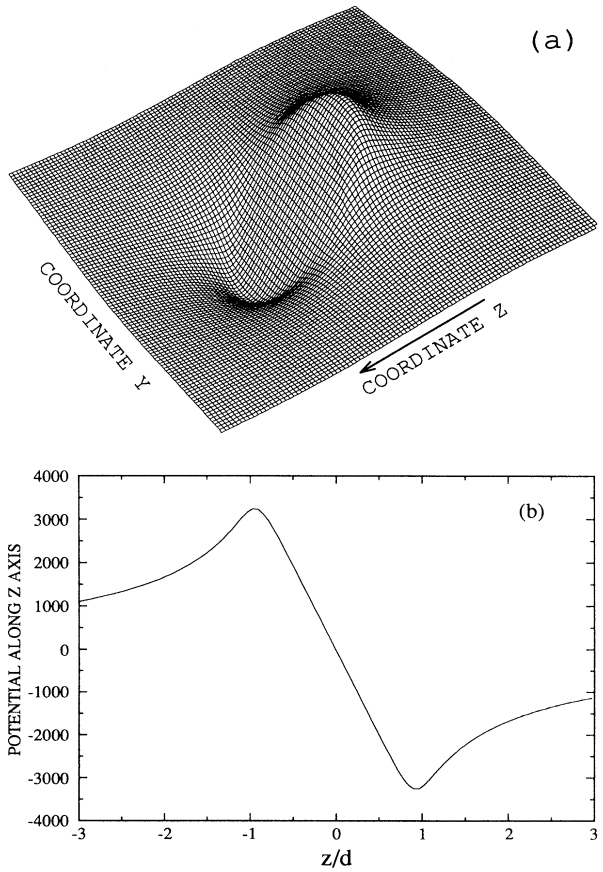

FIG. 3. Electrostatic potential φ, created by a Gaussian beam for the parameters of Fig. 1 (a), and its cross section along axis z (b).

magnitude of the effect is much larger in the experiment. The reason is that Fig. 5 corresponds to the case of an ideal Gaussian beam with very narrow spectrum, whereas in reality the beam spectrum is enriched by relatively low-level noise which is either present in its initial amplitude distribution or due to scattering off imperfections in the medium. Analysis of propagation of such "noisy" beams is beyond the scope of this paper; nevertheless, the shape of the output spectrum in Fig. 5 suggests that the physics of this more complicated situation remains the same.

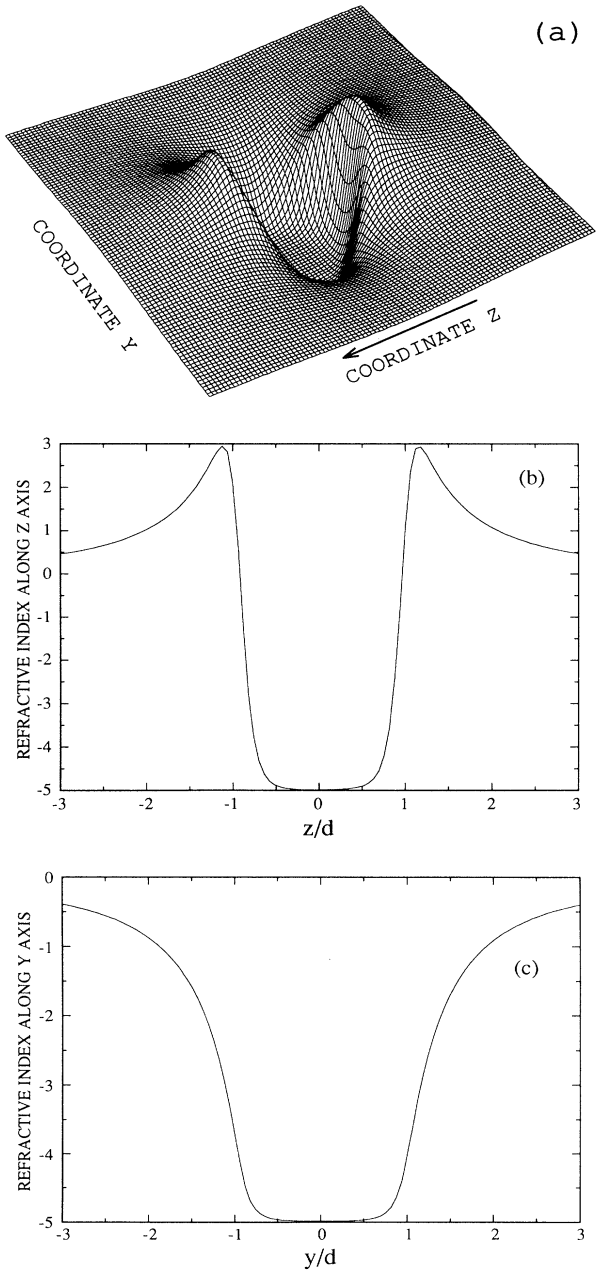

FIG. 4. Nonlinear refractive index, created by a Gaussian beam for the parameters of Fig. 1 (a), and its cross sections along axes z (b) and y (c).

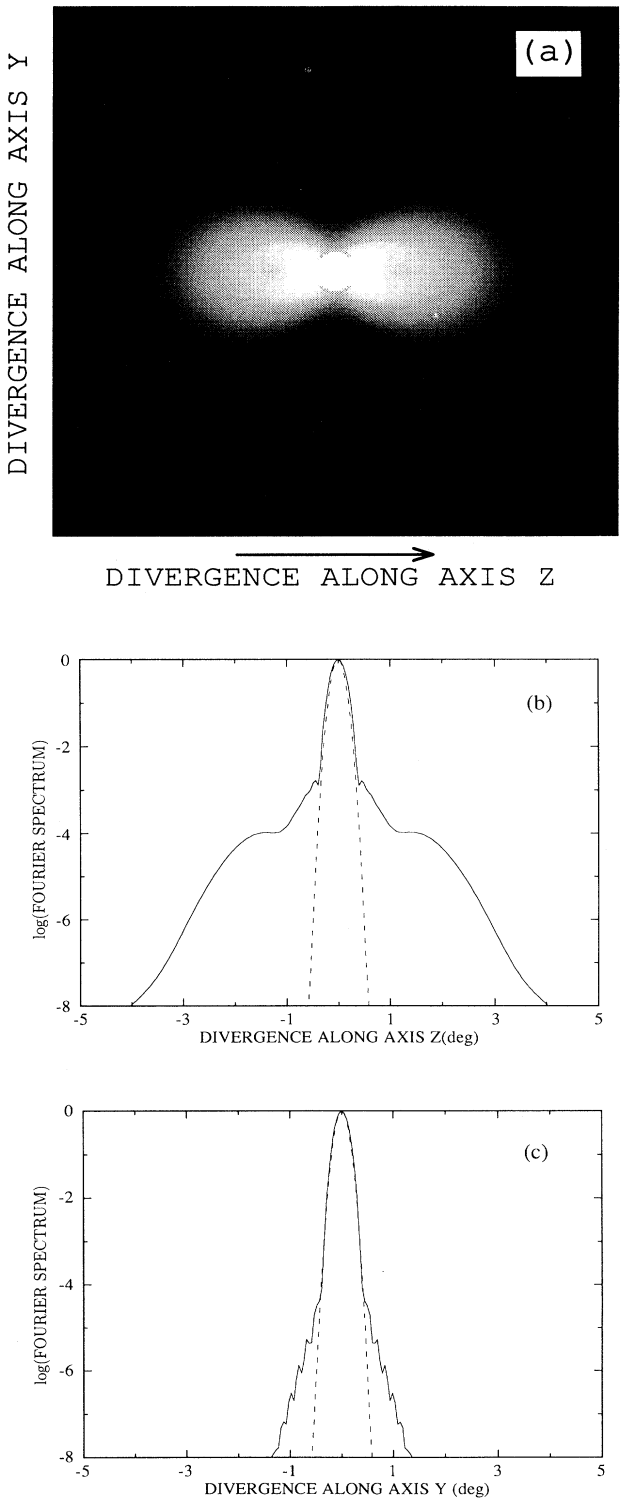

FIG. 5. Output Fourier spectrum of the beam after passing through the medium with the photogalvanic nonlinearity for small values of dark intensity $I_d = 10^{-3}$ (a), and its cross sections along axes z (b) and y (c) ($\log_{10}$ scale). The arrow indicates the direction of the **c** axis. The size of the picture in (a) corresponds to 10° along either direction. The divergence angles are calculated outside the crystal; the divergence angles inside are 2.2 times smaller.

Figure 6 shows the cross section of the potential distribution along the z axis for the case of a light propagating in a photorefractive medium with an applied electric field and with zero photogalvanic field. The calculations are for a Gaussian beam of diameter $d=50$ μm; the field is applied along the c axis and its value is $E_{\text{ext}}=\tilde{E}$. The Debye wave number $k_D/k_0=0.4$, the ratio of components of the electrostatic dielectric tensor $\hat{\epsilon}_y/\hat{\epsilon}_z=2$, $\lambda=514$ μm, and $n=2.3$. The three curves in Fig. 6 correspond to the values of the dark intensity I_d equal to 10^{-5}, 10^{-3}, and 10^{-1}. The distribution of current is very similar to that shown in Fig. 1 except that the net current now flows in the direction of the c axis since we chose $E_{\text{ext}}>0$.

Figure 6 demonstrates that far from the center of the beam where the intensity of light is negligible, the electrostatic field is equal to its externally imposed value E_{ext}. In the region illuminated by the beam this external field is screened by the redistribution of charges, and the net electrostatic field is close to zero. The charge density distribution is very similar to that shown in Fig. 2 except the sign is reversed. Positive charges are now piled up on the positive side of the c axis and negative charges on the negative side. This is caused by our choice of positive sign of an applied electric field; if we invert it, the charge distribution will also invert its sign.

The most important conclusion to be drawn from Fig. 6 is that the amount of screening and, consequently, the magnitude of the electric field in the illuminated region is determined directly by the value of the dark intensity I_d. This parameter is equal to the ratio of the rate of thermal excitation of carriers to the rate of photoexcitation determined by a characteristic intensity of the beam. When this ratio is not very small, some portion of the external electrostatic field penetrates into the illuminated region. When the dark intensity goes to zero, the screening in Fig. 6 is absolute. The amount of screening depends also on the diameter of the beam. The characteristic spatial screening scale, as we have mentioned before, is equal to k_D^{-1}. If the diameter of the beam is extremely small, such that $k_D d \leq 1$, some amount of electric field will penetrate the illuminated region even when the dark conductivity is negligible. Since k_D^{-1} is usually of the order of several wavelengths, the effect of screening holds down to very small diameters of the beam.

Figures 7(a) and 7(b) show the cross sections of the refractive-index distribution along z and y axes, respectively, for the parameters of Fig. 6 ($d=50$ μm). The value of the normalized refractive index for large arguments asymptotically tends to $-E_{\text{ext}}/\tilde{E}$. This uniform background corresponds to the renormalization of the effective wave vector of the light beam and can be sub-

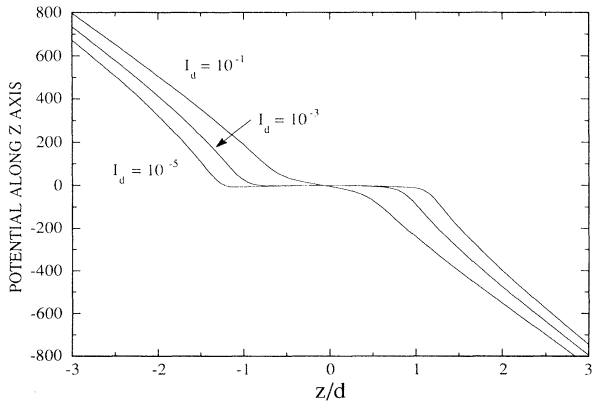

FIG. 6. Cross section of the potential distribution along axis z in the case of an applied electric field for different values of the dark intensity. The diameter of the beam $d=50$ μm, $E_{\text{ext}}=1$, $k_D/k_0=0.4$.

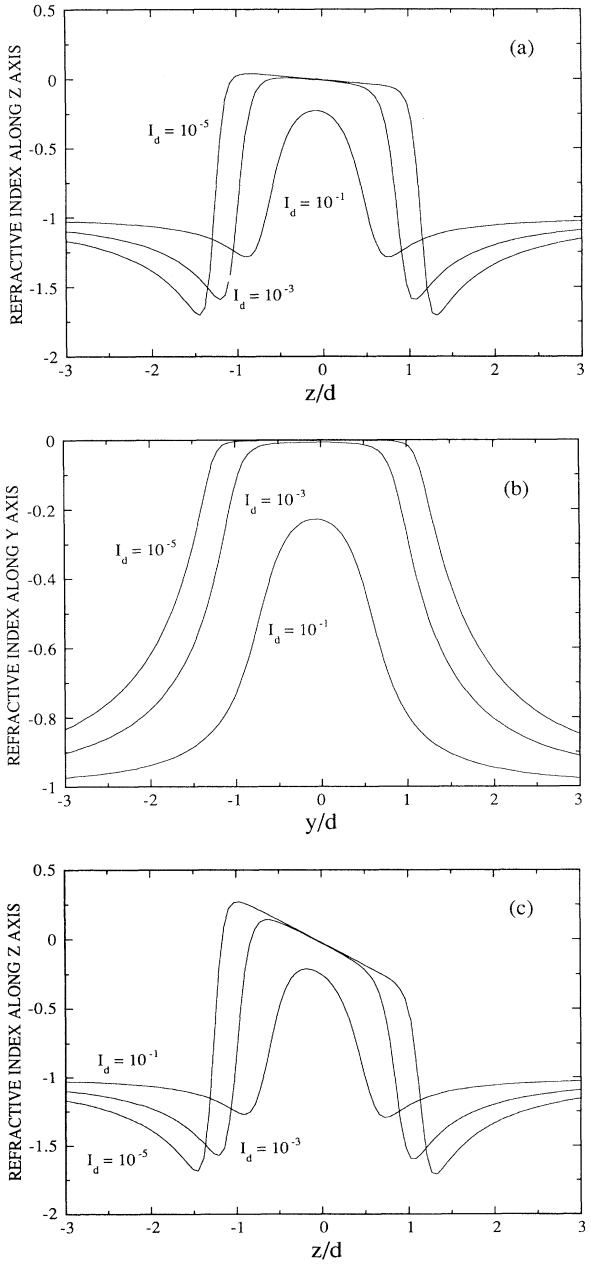

FIG. 7. Cross sections of the refractive index along axes z (a) and y (b) for the parameters of Fig. 6 and the cross section along axis z for five times narrower beam (c).

tracted. The induced changes in the refractive index near the center of the beam (relative to the periphery) are of positive sign. Nevertheless only for large values of the dark intensity ($I_d=10^{-1}$) does this refractive index have a somewhat parabolic shape that can be visualized as a nonlinear focusing lens. For smaller dark intensities the central part of the distribution has linear slope along the z axis and is flat along the y axis. This means that the central part of the beam for small dark intensities does not experience any nonlinear focusing or defocusing, but just bends toward the c axis. At the same time the wings of the beam will undergo strong scattering off sharply changing peripheral regions of the refractive-index distribution. Calculations of the output Fourier spectrum of the beam in this case result in pictures that are qualitatively analogous to those presented in Fig. 5 despite the fact that the sign of the refractive-index change is different.

Another interesting feature of Fig. 7(a) is the linear slope of the curves in the central part. This is a signature of the first term in Eq. (13). Of course this slope is also present in Fig. 4(b), but since the value of the photogalvanic field in Fig. 4(b) is five times larger and the diameter of the beam twice as large as in Fig. 7, its relative magnitude compared to that of the second term in (13) is ten times smaller and thus cannot be clearly seen. Figure 7(c) show the cross section of the refractive index along axis z for a Gaussian beam with the diameter $d=10$ μm. The linear slope in the central part of the distribution is now much more pronounced.

We have already discussed (Fig. 5) the output characteristics of the beam after propagating through a photorefractive medium having low values of the dark intensity. Figure 8 shows the output intensity profile of the input collimated Gaussian beam after propagating through a photorefractive medium having relatively high value of the dark intensity $I_d=10^{-1}$. The initial diameter of the beam is $d=30$ μm, the length of the medium $L=4$ mm, $\hat{\epsilon}_y/\hat{\epsilon}_z=2$, $n=2.3$, $E_{\text{ext}}/\tilde{E}=1$, $k_D/k_0=0.4$, $\lambda=0.633$ μm, and $kn^2r_{33}\tilde{E}L=16$. The Fourier spectrum in this case does not exhibit any small-amplitude high-divergence halo. The near-field output intensity distribution is more informative.

Figure 8(a) shows the cross section of the output intensity profile along the z axis. The solid curve is the output intensity of the beam, the dashed curve is its input intensity, and the dash-dotted curve is the output intensity of the beam without the nonlinearity. The center of the output beam is displaced from its input position. This displacement is due to the symmetric part $\ln I$ of the potential φ in Eq. (13). Figure 8(b) is the slice of the output intensity profile along axis y. The solid, dashed, and dash-dotted curves have the same meaning as in Fig. 8(a). The slices were taken through the maxima of the intensity distributions. Since the output beam has walked off in the z direction, the z coordinate of the solid curve in Fig. 8(b) is different from that of the other two curves. Figures 7 and 8 confirm that for large values of I_d the photorefractive nonlinearity indeed may result in stationary self-focusing. Note that the characteristic width of the output beam along the z direction is less than along y, i.e., the beam is focused preferentially along the axis of spontaneous polarization. The change in sign of the applied electric field E_{ext} results in the self-defocusing of the beam. In the limit of relatively large I_d, photorefractive response has some features in common with the saturable Kerr-type nonlinearity [14], although this analogy cannot be stretched too far.

Figure 8 demonstrates that in propagating through a photorefractive medium, the initially radially symmetric beam becomes elliptical and should be characterized by two principal diameters d_y and d_z determining its widths along the axes y and z, respectively. Figure 9 shows the normalized diameters $f_y(x)=d_y(x)/d$ and $f_z(x)=d_z(x)/d$ (d is the initial diameter of the beam) as functions of the longitudinal coordinate x inside the photorefractive medium for the parameters of Fig. 8. The dashed curve is the normalized diameter of the beam inside the medium in the absence of nonlinearity. In this case $f_y(x)=f_z(x)=\sqrt{[1+(x/l_d)^2]}$, where $l_d=kd^2/8$, so for the parameters of the calculations, the output diameter is about 1.85 times larger than its input value. In the presence of the nonlinearity the beam experiences anisotropic self-focusing. It affects both transverse coordinates, but the magnitude of the effect is different along y and z. Thus the diameter of the beam along the axis y

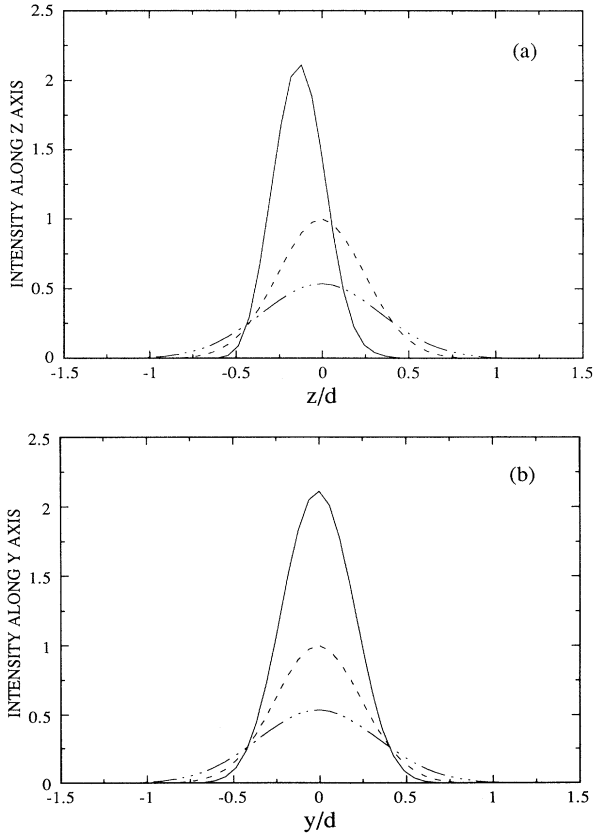

FIG. 8. Output intensity distributions of the beam after passing through the medium with an applied electric field for large value of the dark intensity $I_d=10^{-1}$: (a) the cross section along axis z; (b) the cross section along axis y.

remains approximately equal to its input value. The diameter along the axis z first decreases down to about 0.54 of its input value at $x \approx 2.5$ mm, and then increases again to the output value $f_z(x=l_x) \approx 0.86$. The diameters d_y and d_z in Fig. 9 were calculated according to the formulas: $d_y^2 = 16P^{-1}\int d\mathbf{r}_\perp (y-y_0)^2 \tilde{I}_{\rm em}(\mathbf{r}_\perp)$, where $y_0 = P^{-1}\int d\mathbf{r}_\perp y \tilde{I}_{\rm em}(\mathbf{r}_\perp)$ is the y coordinate of the center of the beam, and $P = \int d\mathbf{r}_\perp \tilde{I}_{\rm em}(\mathbf{r}_\perp)$ is its total power; the same procedure was used for d_z.

Figure 10 presents time evolution of the output diameter of the initially collimated Gaussian beam calculated in the framework of a nonstationary two-dimensional model. It follows from Eqs. (6) and (8) by discarding the transverse coordinate y. All relevant parameters in Fig. 10 are as in Figs. 8 and 9. The time is normalized to the characteristic relaxation time corresponding to the maximum intensity of the input beam. Two curves correspond to the values of the dark intensity I_d equal to 0.1 and 0.01. At zero time the output normalized diameter of the beam equals $f_z \approx 1.85$. As the photorefractive nonlinearity builds up, the beam starts focusing inside the medium and its output diameter decreases. This first stage happens at times of the order of several characteristic relaxation times. After that the output diameter relatively slowly relaxes to its steady state value. This value corresponds to $f_z \approx 0.7$ for $I_d = 0.1$ and to $f_z \approx 1.37$ for $I_d = 0.01$. Figure 9 shows that the initial phase of self-focusing (until about ten relaxation times for the parameters of the calculation) is almost independent of the value of the dark intensity. At larger times, when the charge carries have had time to redistribute themselves, the evolution is directly determined by the value of I_d. The comparison of Figs. 9 and 10 also indicates that the output diameter of the beam as predicted by the two-dimensional model may be considered a reasonable approximation to the results of the full three-dimensional treatment.

Experimental observations of self-focusing of a light beam in a photorefractive medium with an applied electric field were recently reported in Refs. [15,16]. A two-dimensional theoretical model of this phenomenon was published in Ref. [17]. The physical interpretation of the experimental results in [15,16] is contradictory. The theory of Ref. [17] which predicts steady-state self-focusing does not include the dark intensity ($I_d = 0$); on the other hand, experimental results and qualitative analysis in [16] indicate that this dark intensity is necessary and should be large enough. Our analysis confirms the arguments given in Ref. [16] and contradicts the theory of Ref. [17]. The reason for the discrepancy between our results and those of Ref. [17] is as follows: Ref. [17] used a particular solution of linearized two-dimensional versions of Eqs. (2) with the amplitude of a light beam consisting of two plane waves. A general solution for an arbitrary transverse distribution of the beam was assumed to be a linear superposition of such solutions with plane waves being all possible pairs from the Fourier decomposition of the beam amplitude. This assumption is incorrect, as indicated by the analysis of the present paper. For example, the effect of screening was lost.

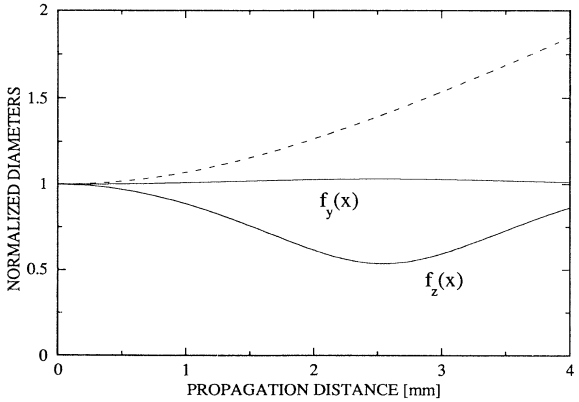

FIG. 9. Normalized diameters of the beam inside the medium for the parameters of Fig. 8.

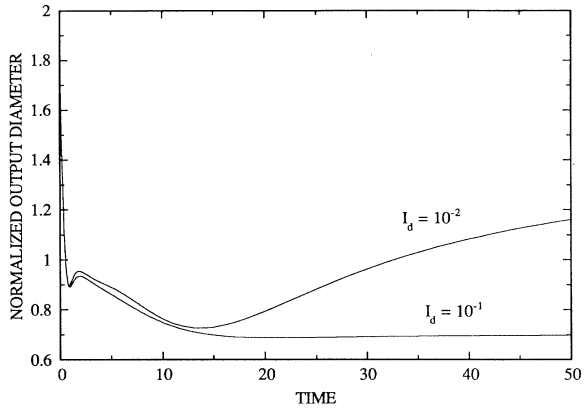

FIG. 10. Time evolution of the output diameter of the beam calculated in the framework of a two-dimensional model for $I_d = 10^{-2}$ and 10^{-1}. All relevant parameters are as in Figs. 8 and 9.

V. CONCLUSIONS

We have considered propagation of a light beam through a photorefractive medium in the framework of a three-dimensional model. We have formulated the set of equations governing three-dimensional distribution of a nonlinear refractive index induced by the optical beam in the medium. It explicitly takes into account the anisotropic nature of the photorefractive medium and allows for the presence of a photogalvanic nonlinearity and/or an externally applied electric field. Solution of these equations involves calculation of a long-range electrostatic potential and requires proper imposition of the boundary conditions, as in any electrostatic problem. We have shown that the most important parameter governing beam propagation through the photorefractive medium in the presence of a photogalvanic nonlinearity and/or an externally applied electric field is the value of the normalized dark intensity I_d. This parameter is the ratio of the rate of thermal excitation of carriers to the rate of pho-

toexcitation determined by a characterization intensity of the beam. In a typical situation I_d is much smaller than unity. Nevertheless it is extremely important that I_d be properly accounted for, since its value determines the shapes of the spatial distributions of charge and electrostatic potential induced by the beam in the medium. It also determines the shape of the nonlinear refractive index and the output spatial and spectral distributions of the beam.

We have shown that in the presence of the photogalvanic effect or an externally applied electric field, propagation of the beam through the medium is accompanied by generation of macroscopic steady-state vortex currents satisfying the equation $\nabla \cdot \mathbf{J}=0$. The magnitude of these currents is proportional to the product of the dark intensity and the value of the photogalvanic or externally applied electric field.

We have calculated and analyzed the distributions of the electric charge, the potential, and the refractive index created by the beam. The underlying physics may be described quite simply as the tendency of the photorefractive medium to counterbalance and screen the action of the photogalvanic term or of the applied electric field. This screening is achieved by a redistribution of charges. These charges accumulate mostly at the periphery of the beam, where its local intensity becomes comparable to the dark intensity. For low values of the dark intensity the screening is nearly absolute in the central part of the beam. The electrostatic potential in this region is equal to the potential that would be created by the beam in the absence of the photogalvanic and/or applied electric field (plus possibly a linearly changing term that uniformly renormalizes the refractive index). The steady-state distribution of the nonlinear refractive index for small values of the dark intensity is characterized by the relatively smooth central part with a slope and by the sharply changing peripheral regions. Propagation of the beam through the medium in such conditions results in a broadening of its spatial spectrum, independent of the sign of the induced refractive index. For relatively large values of the dark intensity I_d the effect of screening is not absolute. The photorefractive nonlinearity in these conditions resembles the conventional saturable Kerr-type nonlinear response. In particular, propagation of the beam through the medium may be accompanied by its stationary self-focusing or defocusing depending on the sign of the induced refractive index. For small values of the dark intensity the beam may experience only transient self-focusing or defocusing.

ACKNOWLEDGMENT

This work was supported by NSF Grant No. PHY90-12244.

[1] *Photorefractive Materials and their Applications 1,* edited by P. Günter and J. P. Huignard (Springer-Verlag, Berlin, 1991).
[2] M. P. Petrov, S. I. Stepanov, and A. V. Khomenko, *Photorefractive Crystals in Coherent Optical Systems* (Springer-Verlag, Berlin, 1991).
[3] J. Feinberg, J. Opt. Soc. Am. **72**, 46 (1982).
[4] A. A. Esayan, A. A. Zozulya, and V. T. Tikhonchuk, Sov. Phys. Lebedev Inst. Rep. **5**, 45 (1990).
[5] O. V. Lybomudrov and V. V. Shkunov, J. Opt. Soc. Am. B **11**, 1408 (1994).
[6] C. Xu, D. Statman, and J. K. McIver, J. Opt. Soc. Am. B **9**, 1825 (1992).
[7] N. V. Kukhtarev, V. B. Markov, S. G. Odulov, M. S. Soskin, and V. L. Vinetskii, Ferroelectrics **22**, 949 (1979).
[8] P. Günter, Phys. Rep. **93**, 200 (1982).
[9] B. Fridkin and B. Sturman, *The Photogalvanic and Photorefractive Effects in Noncentrosymmetric Materials* (Gordon and Breach, New York, 1992).
[10] J. A. Stamper, Laser Part. Beams **9**, 841 (1991).
[11] V. V. Voronov, I. R. Dorosh, Yu. S. Kuz'minov, and N. V. Tkachenko, Kvant. Elektron (Moscow) **7**, 2313 (1980) [Sov. J. Quantum Electron. **10**, 1346 (1980)].
[12] G. D. Bacher, Ph.D. thesis, University of Southern California, 1994.
[13] Q. W. Song, C. Zhang, and P. Talbot, Appl. Opt. **32**, 7266 (1993).
[14] M. Karlsson, Phys. Rev. A **46**, 2726 (1992).
[15] G. C. Duree *et al.*, Phys. Rev. Lett. **71**, 533 (1993).
[16] M. D. Iturbe Castilio, P. A. Marques Aguilar, J. J. Sanches-Mondragon, S. Stepanov, and V. Vysloukh, Appl. Phys. Lett. **64**, 408 (1994).
[17] M. Segev, B. Crossignani, A. Yariv, and B. Fischer, Phys. Rev. Lett. **68**, 923 (1992); B. Crossignani, M. Segev, D. Engin, P. DiPorto, A. Yariv, and G. Salamo, J. Opt. Soc. Am. B **10**, 446 (1993).

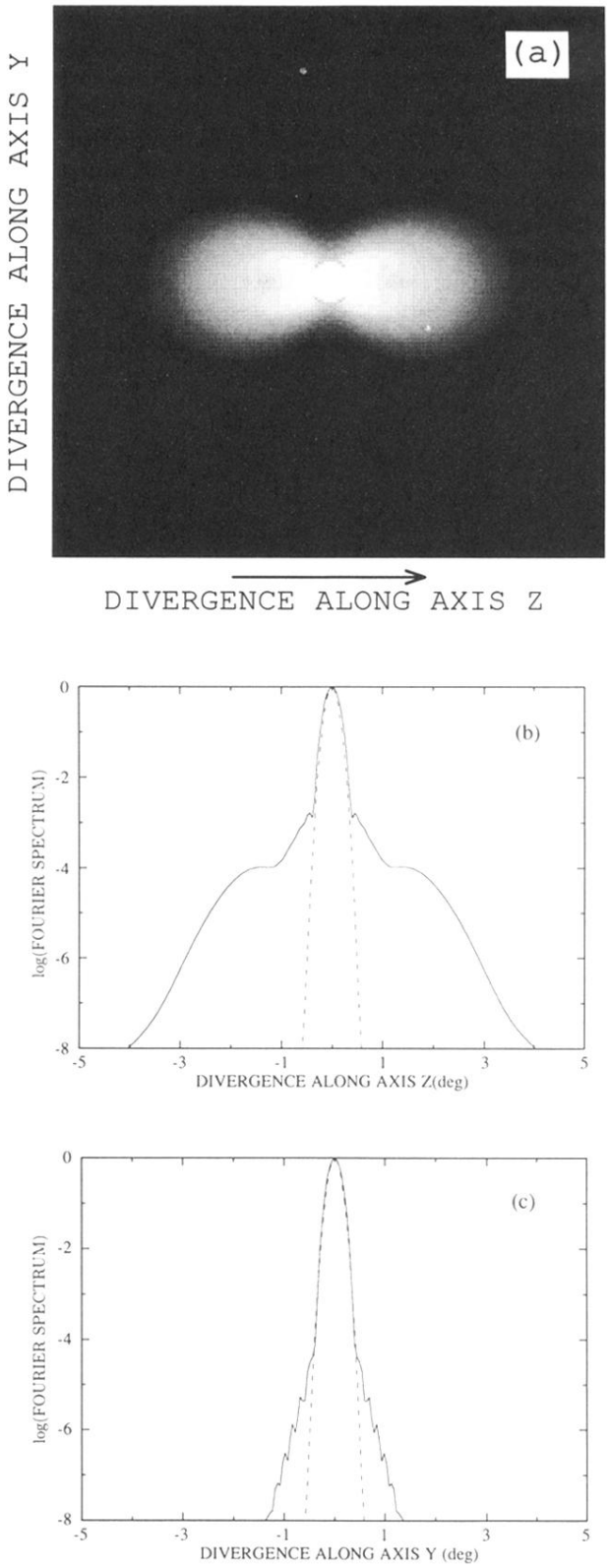

FIG. 5. Output Fourier spectrum of the beam after passing through the medium with the photogalvanic nonlinearity for small values of dark intensity $I_d = 10^{-3}$ (a), and its cross sections along axes z (b) and y (c) ($\log_{10}$ scale). The arrow indicates the direction of the **c** axis. The size of the picture in (a) corresponds to 10° along either direction. The divergence angles are calculated outside the crystal; the divergence angles inside are 2.2 times smaller.